Educational Administration: Theory and Practice
2024, 30(1), 6247-6257
ISSN: 2148-2403
https://kuey.net/

Research Article

Extending Λcdm Cosmology In Presence Of Curvature And Anisotropy: A Model Comparison

Vikrant Yadav[1], Rajpal[2*]

[1,2*]School of Basic and Applied Sciences, Raffles University, Neemrana - 301705, Rajasthan, India.

***Corresponding Author:** Rajpal
[a]rajpal05041985@gmail.com

Citation: Rajpal, et.al (2024). Extending Λcdm Cosmology In Presence Of Curvature And Anisotropy: A Model Comparison, *Educational Administration: Theory and Practice*, 30(1) 6247-6257
Doi: 10.53555/kuey.v29i3.9645

ARTICLE INFO

ABSTRACT

In this work, we present observational constraints on the most anisotropic extensions of the standard ΛCDM model namely ΛCDM+$\Omega_{\kappa 0}$, ΛCDM+$\Omega_{\kappa 0}$ +$\Omega_{\sigma 0}$, $wCDM + \Omega_{\kappa 0}$, wCDM+$\Omega_{\kappa 0}$ +$\Omega_{\sigma 0}$ based on observational data such as SHoES Cepheid host distance anchors, Big Bang Nucleosynthesis (BBN), Pantheon Plus (PP) compilation of Supernovae Type Ia (SNe Ia), Baryon Acoustic Oscillations (BAO), and Cosmic Chronometers (CC). In every analysis, the top bounds on the anisotropy are around 10^{-13} at 95% CL. In every instance including both data combinations, the quintessence behavior of dark energy is preferred at 68% CL. H_0 = 72.25 ± 0.84 km s^{-1} Mpc^{-1} in the wCDM+$\Omega_{\kappa 0}$ +$\Omega_{\sigma 0}$ model and H_0 = 72.48 ± 0.89 km s^{-1} Mpc^{-1} in the ΛCDM+$\Omega_{\kappa 0}$ +$\Omega_{\sigma 0}$ model, both at 68% CL, are the highest values of the Hubble constant found in the analysis.

Keywords: dark energy, cosmological constant, curvature, anisotropy

I.INTRODUCTION

'Over' the last few decades, the scientific community has embraced Lambda CDM as the standard model in cosmology based on the theory of inflation [1–4]. It describes the universe on vast scales through the spatially flat Friedmann-Lemaˆıtre-Robertson Walker (FLRW) spacetime metric, which is a homogeneous, isotropic, and flat Robertson-Walker (RW) spacetime metric. Meanwhile, General Relativity (GR) is used to describe the dynamics of the universe. This model has excellent agreement with a wide range of observational data from various regions of the universe[5–12]. Nevertheless, recent studies have detected certain inconsistencies in the numerical values of specific cosmological parameters [13, 14], a significant matter of concern within cosmology and the domain of theoretical physics. It could suggest the need for new physics beyond the established fundamental theories, extending the ΛCDM model.

Firstly, we summarize spatially curvature (flat or non-flat) within the generalized of ΛCDM model. In the past few years, the cosmic community was not sure about the curvature of the universe, whether it is flat or not [15] but some observational evidence has supported that the universe is spatially flat [16–21]. However, a detailed [7] analysis of the CMB temperature and polarization data using Planck satellite observations suggested that a closed universe (with Ω_κ = −0.044+0.018−0.015 for TT, TE, EE+lowE) was preferred, with a statistical significance of about 3σ. This conclusion is supported not only by the low CMB anisotropy quadrupole but also by WMAP CMB and Effective Field Theories of Large-Scale Structure with Baryon Acoustic Oscillations (BAO) data [22, 23]. When combining Planck CMB data with astrophysics data such as BAO, cosmic chronometers (CC), and type Ia Supernovae (SNIa), diminishes the significance of favoring a closed universe [24–28]. Additionally, as per the analysis in [29] demonstrated that Ω_κ = 0.078+0.086 −0.099 could only be obtained from Sloan Digital Sky Survey's BAO measurements, combined with baryon density and CMB monopole temperature. In fact, the observations indicating a small curvature cannot be considered as evidence for a spatially flat universe in the absence of a solid theoretical argument [30] and the assumption of spatial flatness instead of spatial curvature could lead to significant changes in cosmological parameters [31]. We are curious to explore the impact of considering the curvature of the universe on the current cosmological tensions and free parameter of the dark energy.

The Hubble constant (H_0) is a crucial parameter within modern cosmology that delineates the universe's expansion rate. However, there has been a significant debate and interest in recent years regarding the precise value of H_0. Several observation methods have led to slightly different results, which has caused tensions in determining H_0, known as Hubble tension. This tension refers to the most statistically significant disagreement at 5.0σ between the Planck collaboration value of $H_0 = 67.27 \pm 0.60$ km s^{-1} Mpc^{-1} at a 68% confidence level (CL),[7] assumed by the ΛCDM, and SH0ES collaboration constraint value of $H_0 = 73.27 \pm 1.04$ km s^{-1} Mpc^{-1} at a 68% CL, based on the supernovae calibrated by Cepheids [32]. In addition, there are several late-time measurements that suggest a higher value for the Hubble constant, which is in disagreement with the Planck-CMB estimate. For instance, the Megamaser Cosmology Project [33] found $H_0 = 73.9 \pm 3.0$ km s^{-1} Mpc^{-1}, while the Surface Brightness Fluctuations [34] gave a value of $H_0 = 73.3 \pm 2.4$ km s^{-1} Mpc^{-1}. However, The Planck-CMB data suggests a lower value of H_0, which is consistent with the constraints of BAO and Big Bang Nucleosynthesis (BBN), alongside corroborative evidence from other CMB experiments like ACT-PolDR4 [35], ACT-PolDR6 [36], and SPT-3G [37]. This disparity has been widely discussed in the literature and could indicate the existence of novel physics outside the standard model of cosmology[25, 28, 38–41]. There are several extensions of ΛCDM proposed to address the H_0 tension, such as decaying DM[42–45], DM-DE interactions[46 –50], introducing early DE, and introducing a sign-switching DE at intermediate redshifts (z ~2)[51–54]. Recent review articles provide more information on the current state of H_0 tension and possible solutions[13, 55].

Further, we now discuss the expansion anisotropy and its consequences in terms of the present-day density parameter, denoted $\Omega_{\sigma 0}$. The Wilkinson Microwave Anisotropy Probe (WMAP) experiment first observed that the slight fluctuations in the CMB from various directions of the sky [56] and other observational data sets such as Gamma Ray Bursts (GRBs), Quasars, Galaxies, and SNe Ia also support this finding. These fluctuations have been statistically observed to be of the order ~ 10^{-9}, as stated in reference [57], after analyzing the temperature anisotropy data from the Planck Legacy. The model-independent upper bound of the current expansion anisotropy density parameter is of order ~ 10^{-3} from type Ia supernovae [58–60]. This upper bound is consistent with model-dependence using the combination of H(z) and SNIa data [61, 62]. Generally, the model-dependent upper bounds are much tighter in the range from 10^{-11} to 10^{-23}. In [53], the upper bound of the anisotropy density parameters is constrained to be the order of ~ 10^{-2} from the combined H(z) and SnIa Pantheon data set. However, this constraint becomes even tighter, up to the orders of ~ 10^{-17}, when considering the combined CMB+BAO data set. A similar investigation is carried out in [63] by considering anisotropic expansion. The upper limit is usually strongly constrained by combining the CMB data sets with other cosmological datasets. However, some studies in the literature have shown that the upper limit of the anisotropy parameter can reach an approximation of ~ 10^{-14}[63, 64], even with a CMB independent combination of the data sets.

We are motivated by a recent [63] on the anisotropy model from various combinations of BAO, BBN, CC, PP, and SH0ES data sets. This study has hinted that the drag redshift could be treated as a free parameter, which is closely associated with the Hubble tension and may alleviate it. In this work, our aim is to investigate how the spatial curvature of the universe affects on other cosmological parameters and to constrain the Hubble parameter by utilizing a different set of data combinations. The structure of the paper can be summarized as follows: In the next section, we have discussed the FLRW spacetime metric, Bianchi-type space-time metric and the cosmological models under consideration, while in section III, we present the complete overview of the observational dataset and analysis methodology. After that, in section IV, we present the results and discuss findings of this analysis. Finally, we conclude with a summary of our work in section V.

II.FORMULATING EQUATIONS AND MODELS

In the present section, we shall discuss the spacetime metrics, namely, FLRW metric, Bianchi type-I metric. These metrics have the property of spatial homogeneity but not necessarily isotropy. Also, we shall calculate the Ricci scalar and anisotropic parameter for each metric and define the corresponding models in the final subsection.

➔ FLRW spacetime metric

Consider the FLRW metric, which can be formulated in cartesian coordinates as follows:

$$ds^2 = -dt^2 + s^2 \frac{dx^2+dy^2+dz^2}{[1+\frac{\kappa}{4}(x^2+y^2+z^2)]^2} \qquad (1)$$

where κ represents the curvature scalar, which represents open, flat, and closed universes with κ < 0, κ = 0 and κ > 0, respectively. Also, the Einstein's field equations from General Relativity, are given by

$$G_{\mu\nu} \equiv R_{\mu\nu} - \frac{1}{2} g_{\mu\nu} R = 8\pi G T_{\mu\nu}\,, \qquad (2)$$

where $G_{\mu\nu}$, $R_{\mu\nu}$, R, and $g_{\mu\nu}$ are representing Einstein tensor, Ricci tensor, Ricci scalar, and metric tensor, respectively. Again, on the right hand side, G, and $T_{\mu\nu}$ are representing Newton's gravitational constant and energy-momentum tensor, respectively. The most commonly used form of the total energy-momentum tensor for a perfect fluid is:

$$T^{\nu}{}_{\mu} = \text{diag}[-\rho, p, p, p]. \qquad (3)$$

As a consequence of the twice-contracted Bianchi identity, that is, $G^{\mu\nu}{}_{;\nu} = 0$, the Einstein's field equations (2)satisfy the conservation equation which is as follows:

$T^{\mu\nu}{}_{;\nu} = 0.$ (4)

Further, for a perfect fluid matter distribution, (4) simplifies to

$\dot{\rho} + 3H(1 + w)\rho = 0,$ (5)

where the overdot represents a derivative of the parameter with respect to the cosmic time t. For a perfect fluid i, with pressure p_i, energy density ρ_i, and constant equation of state (EoS) defined by $w_i = p_i/\rho_i$, the continuity equation (5) describes the evolution of its energy density as follows:

$\rho_i = \rho_{io} s^{-3(1+wi)},$ (6)

where ρ_{io} represents the present-day value of ρ_i, corresponding to $s = s_o = 1$, the present-day value of the scale factor. The subscript 'o' attached to any quantity denotes its value in the present-day Universe. We assume that the presence of standard cosmological components in the Universe, such as radiation (consisting of photons and neutrinos) characterized by EoS parameter $w_r = p_r/\rho_r = 1/3$, pressureless fluid (including baryonic and cold dark matter) with EoS $w_m = p_m/\rho_m = 0$, and EoS of dark energy denoted as w_{deo} to be fixed by observations in the analysis. These energy constituents interact only through gravity. As a consequence, each energy source independently satisfies the continuity equation (5), and considering (6), this leads to

$\rho \equiv \rho_r + \rho_m + \rho_{deo} = \rho_{ro} s^{-4} + \rho_{mo} s^{-3} + \rho_{deo} s^{-3(1+w deo)}.$ (7)

Now, Einstein's gravitational equation (2) for the FLRW metric (1) leads to the differential equation is given by

$3\frac{\dot{s}^2}{s^2} = 8\pi G\rho - 3\frac{\kappa}{s^2}$ (8)

$-2\frac{\ddot{s}^2}{s^2} - \frac{\dot{s}^2}{s^2} = 8\pi G p - \frac{\kappa}{s^2}$ (9)

Here, the shear scalar ($\sigma^2 = 0$) and Ricci scalar ($R = 6\kappa s^{-2}$) are derived from FLRW metric (2).

➔ Bianchi type-I spacetime metric

Further, we can formulate a spatially flat, homogeneous, and anisotropic universe through the Bianchi type-I spacetime metric. This metric introduces different scale factors along three orthogonal directions can be written as

$ds^2 = -dt^2 + A^2dx^2 + B^2dy^2 + C^2dz^2,$ (10)

where $\{A, B, C\}$ represent the directional scale factors along three different spatial directions $\{x, y, z\}$, each being a function of cosmic time t only. The corresponding average expansion scale factor: $s = (ABC)^{\frac{1}{3}}$, arising from the average Hubble parameter: $H = \frac{\dot{s}}{s} = \frac{1}{3}(H_x + H_y + H_z)$, where $H_x = \frac{\dot{A}}{A}$, $H_y = \frac{\dot{B}}{B}$, and $H_z = \frac{\dot{C}}{C}$ are the directional

Hubble parameters defined three along different spatial directions {x, y, z}.

We obtained the following set of differential equations by Einstein's gravitational equation (2) for the Bianchi type-I metric (10):

$\frac{\dot{A}}{A}\frac{\dot{B}}{B} + \frac{\dot{B}}{B}\frac{\dot{C}}{C} + \frac{\dot{A}}{A}\frac{\dot{C}}{C} = 8\pi G\rho,$ (11)

$-\frac{\ddot{B}}{B} - \frac{\ddot{C}}{C} - \frac{\dot{B}}{B}\frac{\dot{C}}{C} = 8\pi G p,$ (12)

$-\frac{\ddot{A}}{A} - \frac{\ddot{C}}{C} - \frac{\dot{A}}{A}\frac{\dot{C}}{C} = 8\pi G p,$ (13)

$-\frac{\ddot{A}}{A} - \frac{\ddot{B}}{B} - \frac{\dot{A}}{A}\frac{\dot{B}}{B} = 8\pi G p.$ (14)

The shear scalar expressed through directional Hubble parameters reads:

$\sigma^2 = \frac{1}{6}[(H_y - H_x)^2 + (H_z - H_y)^2 + (H_x - H_z)^2].$ (15)

The equations (12)-(14) can be recast in terms of directional Hubble parameters as follows:

$\dot{H}_x - \dot{H}_y + 3H(H_x - H_y) = 0,$ (16)

$\dot{H}_y - \dot{H}_z + 3H(H_y - H_z) = 0,$ (17)

$\dot{H}_z - \dot{H}_x + 3H(H_z - H_x) = 0.$ (18)

The equation governing shear propagation is derived by the time derivative of σ^2 in Eq. (15) along with these equations (16)-(18) reads as:

$\dot{\sigma} + 3H\sigma = 0,$ (19)

which on integration yields

$\sigma^2 = {\sigma_0}^2 s^{-6}.$ (20)

Here, the Ricci scalar is null for Bianchi type-I spacetime metric (10).

➔ MODELS

The generalized Friedmann equation for the non-flat, homogeneous, and anisotropic spacetime metric with non-tilted perfect fluids is written as:

$3H^2 = 8\pi G(\rho + \rho_\kappa + \rho_\sigma),$ (21)49

where ρ represents the energy density of universe given in equation (7), while ρ_κ, ρ_σ stand for the energy densities of spatial curvature and expansion anisotropy respectively. These are given by:

$\rho_\kappa = \frac{R-1}{2}\frac{1}{8\pi G}$, $\rho_\sigma = \frac{\sigma^2}{8\pi G}$. (22)50

Using Equations (7), (49), and (50), we derive the comprehensive Friedmann equation for a non-flat, homogeneous, and anisotropic spacetime metric with non-tilted perfect fluids:

$\frac{H^2(s)}{{H_0}^2} = \Omega_{\sigma 0}s^{-6} + \Omega_{r0}s^{-4} + \Omega_{m0}s^{-3} + \Omega_{\kappa 0}s^{-2} + \Omega_{de0}s^{-3(1+w_{de0})}$. (23)51

Here, $\Omega_{\sigma 0}$ represents the expansion anisotropy parameter, which is non-negative, while Ω_{r0}, Ω_{m0}, $\Omega_{\kappa 0}$ and Ω_{de0} denote the radiation, matter, curvature, and dark energy density parameters, respectively. These parameters satisfy the equation:

$\Omega_{\sigma 0} + \Omega_{r0} + \Omega_{m0} + \Omega_{\kappa 0} + \Omega_{de0} = 1$. (24)

The absolute CMB monopole temperature, T_o=2.7255±0.0006 K, measured by FIRAS, provides precise constraints on the present-day radiation energy density, expressed as:

$\Omega_{r0} \equiv \frac{\rho_{r0}}{3{H_0}^2} = 2.469 \text{ x } 10^{-5}h^{-2}(1 + 0.2271N_{eff})$. (25)

Here, h=H_o/(100 km s^{-1}Mpc^{-1}) and N_{eff}=3.046 represents the standard number of effective neutrino species with a minimum allowed mass of m_ν= 0.06 eV.

The generalized Friedmann eq. (51) describes a non-flat, homogeneous, and anisotropic universe, denoted by wCDM+$\Omega_{\kappa 0}$ +$\Omega_{\sigma 0}$ with the set of free parameters $P_{w\text{CDM}+\Omega_{\kappa 0}+\Omega_{\sigma 0}}$ ={ω_b, ω_c, H_o, $\Omega_{\sigma 0}$, $\Omega_{\kappa 0}$, w_{de0}}. When there is no expansion anisotropy present in eq.(51) then this equation reduces to the form:

$\frac{H^2(s)}{{H_0}^2} = \Omega_{r0}s^{-4} + \Omega_{m0}s^{-3} + \Omega_{\kappa 0}s^{-2} + \Omega_{de0}s^{-3(1+w_{de0})}$, (26)

which shall be denoted by wCDM+$\Omega_{\kappa 0}$ model with the set of free parameters $P_{w\text{CDM}+\Omega_{\kappa 0}}$ ={ω_b, ω_c, H_o, $\Omega_{\kappa 0}$, w_{de0}}.

Again, if the value of the EoS parameter of dark energy, w_{de0} , is equal to -1, that is, the cosmological constant form of dark energy, then the above anisotropic model reduces to the form:

$\frac{H^2(s)}{{H_0}^2} = \Omega_{\sigma 0}s^{-6} + \Omega_{r0}s^{-4} + \Omega_{m0}s^{-3} + \Omega_{\kappa 0}s^{-2} + \Omega_{\Lambda 0}$, (27)

where $\Omega_{\Lambda 0}$ represents the cosmological constant form of dark energy. This model shall be denoted by ΛCDM+$\Omega_{\kappa 0}$ +$\Omega_{\sigma 0}$ with the set of free parameters $P_{\Lambda\text{CDM}+\Omega_{\kappa 0}+\Omega_{\sigma 0}}$ ={ω_b, ω_c, H_o, $\Omega_{\sigma 0}$, $\Omega_{\kappa 0}$ }. When there is no expansion anisotropy present in eq.() then it reduces to the form:

$\frac{H^2(s)}{{H_0}^2} = \Omega_{r0}s^{-4} + \Omega_{m0}s^{-3} + \Omega_{\kappa 0}s^{-2} + \Omega_{\Lambda 0}$, (28)

which shall be denoted by ΛCDM+$\Omega_{\kappa 0}$ model with the set of free parameters $P_{\Lambda\text{CDM}+\Omega_{\kappa 0}}$ ={ω_b, ω_c, H_o, $\Omega_{\kappa 0}$ }.

III.DATASETS AND METHODOLOGY

Following data sets have been used this work:

➔ Baryon Acoustic Oscillations (BAO)

We analyze 14 BAO measurements obtained from the final dataset of the Sloan Digital Sky Survey (SDSS) [9]. These measurements provide independent constraints on angular-diameter distances and Hubble distances relative to the sound horizon, derived from eight distinct tracers, including galaxies, quasars, and Lyman- (Lyα) forests.

The comoving size of the sound horizon at the drag epoch (z_d) is expressed as:

$r_d = r_s(z_d) = \int_{z_d}^{\infty} \frac{c_s\, dz}{H(z)}$, (29)

where the sound speed of the baryon-photon plasma is given by:

$c_s = \frac{c}{\sqrt{3(1+R)}}$, with $R = \frac{3\Omega_{b0}}{4\Omega_{\gamma 0}(1+z)}$. (30)

Here, Ω_{b0} = 0.022h^{-2} and $\Omega_{\gamma 0}$ = 2.469 × 10$^{-5}h^{-2}$ represent the present-day physical densities of baryons and photons, respectively, while h = H_o/100 denotes the reduced Hubble parameter [64, 65].

Unlike previous studies [61, 66], which assumed a fixed z_d, our approach follows [63], allowing z_d to vary in BAO data analyses for improved flexibility in model constraints.

➔ Cosmic Chronometer (CC)

We use CC data of 33 $H(z)$ measurements spanning over the redshift values from 0.07 to 1.965 [67-74], which provide a basic relationship between cosmic time t, redshift z, and the Hubble parameter $H(z)$ [75]: $H(z) = -\frac{1}{1+z}\frac{dz}{dt}$.

➔ Big Bang Nucleosynthesis (BBN)

We employ an updated BBN estimate of the physical baryon density, ω_b (where $\omega_b \equiv \Omega_b \ h^2$) from experimental nuclear physics at the Laboratory for Underground Nuclear Astrophysics (LUNA) of the INFN Laboratori Nazionali del Gran Sasso in Italy [76], with a value of 0.02233 ± 0.00036.

➔ Pantheon+ and SHoES

We use the distance moduli measurements obtained from the supernovae of Type Ia (SNe Ia). The theoretical apparent magnitude mB of a supernova at redshift z reads:

$$m_B = 5log_{10}[\frac{d_L(z)}{1Mpc}] + 25 + M_B \qquad (31)$$

where M_B is the absolute magnitude, and $d_L(z)$ is the luminosity distance. We utilize SNe Ia distance modulus data from the Pantheon+ sample [77] with 1701 light curves corresponding to 1550 distinct supernovae Ia in the redshift range of $z \in [0.001, 2.26]$, and refer to this collection as PP. When we incorporate the SHoES Cepheid host distance anchors [77] into our analyses, we refer to this dataset as PPSHoES.

We use uniform priors: $\omega_b \in [0.01, 0.03]$, $\omega_c \in [0.05, 0.25]$, $H_o \in [60, 80]$, $w_{deo} \in [-2, 0]$, $\Omega_{\kappa 0} \in [-0.3, 0.3]$, $\Omega_{\sigma 0} \in [0, 0.001]$. Employing the aforementioned datasets, viz., BAO, CC, BBN, PP and PPSHoES, we obtain the correlated Monte Carlo Markov Chain (MCMC) samples from the interface of MontePython [78] with the publicly available Boltzmann code CLASS [79]. Further, the MCMC samples are further analyzed using the python package GetDist [80].

IV.RESULTS AND DISCUSSIONS

Table I presents the free and derived cosmological parameters for the ΛCDM+$\Omega_{\kappa 0}$ and ΛCDM+$\Omega_{\kappa 0}$ +$\Omega_{\sigma 0}$ models at a 68% CL, obtained from two different combinations of observational data, namely BAO+CC+BBN+PP and BAO+CC+BBN+PPSHoES. The physical baryon density quantity is represented by the baryon density parameter, $10^{-2}\omega_b$, which varies between 2.228 and 2.241 in these two models under the considered datasets. The ΛCDM+$\Omega_{\kappa 0}$ and ΛCDM+$\Omega_{\kappa 0}$ +$\Omega_{\sigma 0}$ models predict different amounts of matter using the two data combinations mentioned above. The cold dark matter density parameter, ω_c, which quantifies the cold dark matter density percentage, ranges from 0.217 to 0.295. The anisotropy parameter, $\Omega_{\sigma 0}$, constrains deviations from mainstream cosmological models by providing upper bounds of $< 3.60 \times 10^{-13}$ and $< 3.90 \times 10^{-13}$. The impact of curvature on the geometry of the cosmos is reflected in the wide range of values of the curvature density parameter, $\Omega_{\kappa 0}$, which ranges from -0.084 ± 0.029 to $0.141^{+0.054}_{-0.063}$. The cosmic expansion rate is measured by the Hubble constant, H_0 , which varies amongst dataset combinations with values ranging from 67.3 ± 1.6 to 72.48 ± 0.89 km s^{-1} Mpc^{-1}. The intrinsic brightness of Type Ia supernovae is described by their absolute magnitude, or M_B, which varies from -19.439 ± 0.049 to -19.284 ± 0.024. Also, the matter density parameter, Ω_{m0}, which represents the current total matter density, varies between 0.266 and 0.340. The range of 1058.2 ± 1.2 to 1062.43 ± 0.89 is the decoupling redshift, z_d, the redshift at which matter and radiation dissociated. The scale of baryon acoustic oscillations (BAO) is characterized by the sound horizon at decoupling, r_d, which ranges from 137.8 ± 1.9 to 147.6 ± 3.3. The models' goodness of fit is indicated by the minimum chi-square (χ^2_{min}) values, which vary from 1322.78 to 1438.28.

The results in Table I demonstrate that the addition of $\Omega_{\kappa 0}$ and $\Omega_{\sigma 0}$ has a considerable effect on the cosmological parameter estimations. With certain dataset combinations suggesting somewhat closed or open universes, the variance in $\Omega_{\kappa 0}$ suggests that there is continuous debate regarding the curvature of the universe. The limitations on $\Omega_{\sigma 0}$ demonstrate that deviations from normal isotropy are negligible, supporting the assumptions of the traditional ΛCDM model. H_0 values were different for the two dataset combinations; the BAO+CC+BBN+PPSHoES combination had a higher value (~72 km s^{-1} Mpc^{-1}) than the BAO+CC+BBN+PP combination (~67 km s^{-1} Mpc^{-1}). This gap is consistent with the ongoing Hubble tension, where measurements from early- and late-universe probes do not completely align. Ω_{m0} is consistently lower in the models that include $\Omega_{\kappa 0}$ and $\Omega_{\sigma 0}$, indicating that these factors might affect the estimation of the total matter composition of the

Table I. The free and some derived parameters of the ΛCDM+$\Omega_{\kappa 0}$ and ΛCDM+$\Omega_{\kappa 0}$ +$\Omega_{\sigma 0}$ models at 68% CL from BAO+CC+BBN+PP and BAO+CC+BBN+PPSHoES combinations of data are constrained (mean values with 68% CL errors). The 95% CL upper bounds for $\Omega_{\sigma 0}$ are shown. The measurement unit for the Hubble constant H_0 is km s^{-1}Mpc^{-1}.

Data set	BAO+CC+BBN+PP		BAO+CC+BBN+PPSHoES	
	ΛCDM+$\Omega_{\kappa 0}$	ΛCDM+$\Omega_{\kappa 0}$ + $\Omega_{\sigma 0}$	ΛCDM+$\Omega_{\kappa 0}$	ΛCDM+$\Omega_{\kappa 0}$ + $\Omega_{\sigma 0}$
$10^{-2}\omega_b$	2.238±0.036	$2.228^{+0.034}_{-0.039}$	2.241±0.034	2.232±0.036
ω_c	$0.261^{+0.033}_{-0.034}$	$0.217^{+0.041}_{-0.043}$	$0.295^{+0.025}_{-0.024}$	$0.236^{+0.043}_{-0.044}$
$\Omega_{\sigma 0}$	0	< 3.60 x 10^{-13}	0	< 3.90 x 10^{-13}
$\Omega_{\kappa 0}$	0.026±0.044	$0.141^{+0.054}_{-0.063}$	−0.084±0.029	0.069±0.061
H_0	67.3±1.6	$68.3^{+1.5}_{-1.8}$	72.27±0.85	72.48±0.89
M_B	−19.439±0.049	−19.403±0.050	−19.296±0.023	−19.284±0.024
Ω_{m0}	0.312±0.015	$0.266^{+0.023}_{-0.019}$	0.340±0.012	0.280±0.022
z_d	1059.8±1.2	1058.2±1.2	1062.43±0.89	1060.1±1.2
r_d	147.6±3.3	145.0±3.3	138.9±1.8	137.8±1.9
χ^2_{min}	1438.28	1437.26	1326.56	1322.78

universe. The constraints on r_d and z_d remain within anticipated ranges, further supporting the consistency of conventional cosmological models with empirical data. According to the χ^2_{min} values, the models that include $\Omega_{\kappa 0}$ and $\Omega_{\sigma 0}$ do not considerably reduce the fit, suggesting that the addition of these parameters has no discernible effect on the viability of the cosmological models.

Table II presents the free and derived cosmological parameters for the wCDM+$\Omega_{\kappa 0}$ and wCDM+$\Omega_{\kappa 0}$ +$\Omega_{\sigma 0}$ models at a 68% CL, obtained from two different combinations of observational

Table II. The free and some derived parameters of the wCDM+$\Omega_{\kappa 0}$ and wCDM+$\Omega_{\kappa 0}$ +$\Omega_{\sigma 0}$ models at 68% CL from BAO+CC+BBN+PP and BAO+CC+BBN+PPSHoES combinations of data are constrained (mean values with 68% CL errors). The 95% CL upper bounds for $\Omega_{\sigma 0}$ are shown. The measurement unit for the Hubble constant H_0 is km s^{-1}Mpc^{-1}.

Data set	BAO+CC+BBN+PP		BAO+CC+BBN+PPSHoES	
	wCDM+$\Omega_{\kappa 0}$	wCDM+$\Omega_{\kappa 0}$ + $\Omega_{\sigma 0}$	wCDM+$\Omega_{\kappa 0}$	wCDM+$\Omega_{\kappa 0}$ + $\Omega_{\sigma 0}$
$10^{-2}\omega_b$	2.238±0.035	2.230±0.035	2.240±0.036	2.230±0.036
ω_c	$0.264^{+0.034}_{-0.035}$	$0.221^{+0.044}_{-0.045}$	$0.298^{+0.025}_{-0.026}$	$0.238^{+0.041}_{-0.043}$
$\Omega_{\sigma 0}$	0	< 3.50 x 10^{-13}	0	< 3.90 x 10^{-13}
$\Omega_{\kappa 0}$	−0.069±0.081	0.032±0.086	−0.188±0.066	−0.042±0.081
w_{de0}	$-0.892^{+0.076}_{-0.052}$	$-0.871^{+0.084}_{-0.058}$	$-0.892^{+0.063}_{-0.046}$	$-0.860^{+0.066}_{-0.053}$
H_0	67.2±1.6	68.2±1.7	72.19±0.87	72.25±0.84
M_B	−19.436±0.048	−19.398±0.051	−19.292±0.024	−19.281±0.023

Ω_{m0}	0.265±0.017	0.224±0.023	0.299±0.013	0.239±0.022
z_d	1059.8±1.2	1058.5±1.3	1062.47±0.91	1060.0±1.2
r_d	147.4±3.3	144.6±3.3	138.7±1.9	137.5±1.9
$\chi^2{}_{min}$	1435.4	1434.22	1322.94	1319.06

data, namely BAO+CC+BBN+PP and BAO+CC+BBN+PPSHoES. All scenarios have the same constraints on $10^{-2}\omega_b$, which ranges from 2.230 to 2.240 with very slight differences between models and datasets. The projected matter content for various assumptions is reflected in the variation of ω_c, which ranges from 0.221 to 0.298. With upper bounds of $< 3.50 \times 10^{-13}$ and $< 3.90 \times 10^{-13}$, $\Omega_{\sigma 0}$ is limited, suggesting little departure from the conventional cosmological model. A broad range of values for $\Omega_{\kappa 0}$, from -0.188 ± 0.066 to 0.032 ± 0.086, illustrates how spatial curvature plays its role in the wCDM+$\Omega_{\kappa 0}$ and wCDM+$\Omega_{\kappa 0}$ +$\Omega_{\sigma 0}$ models. A potential dynamical aspect of dark energy is implied by the dark energy

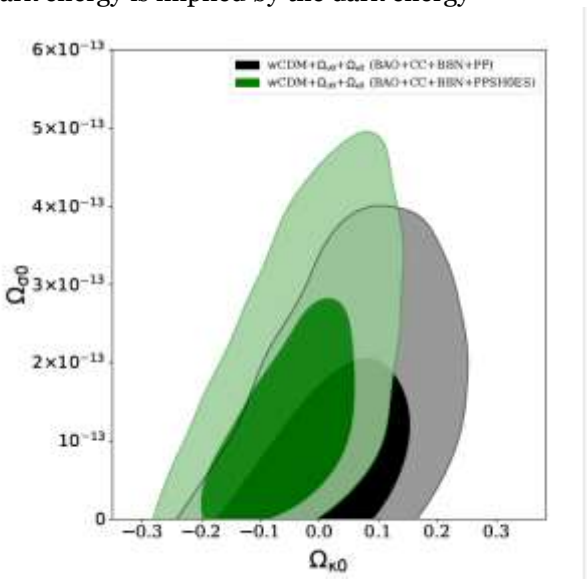

Figure 1: Two-dimensional marginalized confidence regions (at 68% and 95% CL) of $\Omega_{\kappa 0}$- $\Omega_{\sigma 0}$ for wCDM+$\Omega_{\kappa 0}$ +$\Omega_{\sigma 0}$ model from BAO+CC+BBN+PP and BAO+CC+BBN+PPSHoES data combinations.

equation of state parameter, w_{de0} , which deviates from the typical ΛCDM value of -1 and ranges between -0.892 and -0.860. The estimates of H_0 vary from 67.2 ± 1.6 to 72.25 ± 0.84 km s^{-1} Mpc^{-1}, revealing variations in the cosmic expansion rate. Also, M_B varies slightly, ranging from -19.436 ± 0.048 to -19.281 ± 0.023. Variations in model assumptions and dataset combinations are reflected in the range of 0.224 to 0.299 for Ω_{m0} . See Figure 1, Figure 2 and Figure 3 to observe the behaviour of $\Omega_{\kappa 0}$ with other parameters of interest. r_d ranges from 137.5 ± 1.9 to 147.4 ± 3.3, while z_d is restricted to 1058.5 ± 1.3 and 1062.47 ± 0.91. $\chi^2{}_{min}$ ranges from 1319.06 to 1435.4.

We will now carry out the model comparison. Tables I and II show that, in contrast to the ΛCDM model, the wCDM model permits a time-dependent dark energy equation of state, that is, w_{de0} . The values of w_{de0} exhibit slight departures from the conventional cosmological constant assumption w_{de0} = -1 and range from $-0.892^{+0.076}{}_{-0.052}$ to $-0.860^{+0.066}{}_{-0.053}$. In contrast

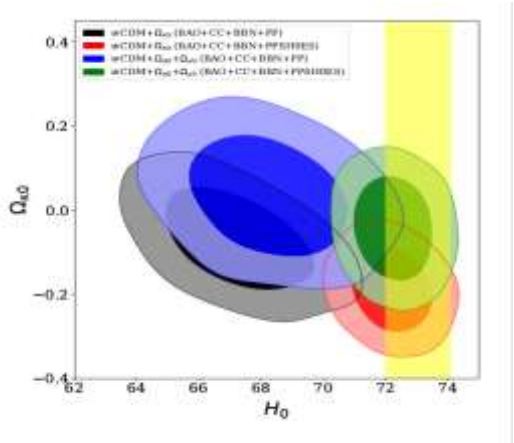

Figure 2: Two-dimensional marginalized confidence regions (at 68% and 95% CL) of H_o- $\Omega_{\kappa 0}$ for wCDM+$\Omega_{\kappa 0}$ and wCDM+$\Omega_{\kappa 0}$ +$\Omega_{\sigma 0}$ models from BAO+CC+BBN+PP and BAO+CC+BBN+PPSHoES data combinations.

to the ΛCDM model, the wCDM model's limits on $\Omega_{\kappa 0}$ show greater variances, ranging from -0.188 ± 0.066 to 0.032 ± 0.086. This implies that under wCDM scenarios, curvature estimations are more sensitive. There are negligible departures from isotropy in both models, as evidenced by the upper bounds on $\Omega_{\sigma 0}$ staying at the same order of magnitude as in ΛCDM. With the BAO+CC+BBN+PPSHoES combination yielding higher values (~72 km s^{-1} Mpc^{-1}) than the BAO+CC+BBN+PP combination (~67 km s^{-1} Mpc^{-1}), the H_o values in the wCDM models stay consistent with those in ΛCDM. The impact of a fluctuating dark energy equation of state on matter content estimate is reflected in the fact that Ω_{m0} in the wCDM models is marginally lower than in ΛCDM, especially in situations with $\Omega_{\kappa 0}$ and $\Omega_{\sigma 0}$ .r_d and z_d in wCDM exhibit values in agreement with ΛCDM, suggesting that changes in the dark energy equation of state do not substantially change these parameters. However, wCDM models have somewhat lower ${\chi^2}_{min}$ values than ΛCDM models, indicating a little better match to the observational evidence.

In general, the wCDM model adds flexibility to the dark energy equation of state, which causes minor differences in estimations of cosmological parameters when compared to ΛCDM. The primary changes are seen in $\Omega_{\kappa 0}$ and Ω_{m0}, where wCDM permits significantly lower matter density values and greater curvature variations. Notwithstanding these variations, the models are largely consistent, supporting the strength of the cosmological constraints in place while providing opportunity for future improvements in dark energy modeling.

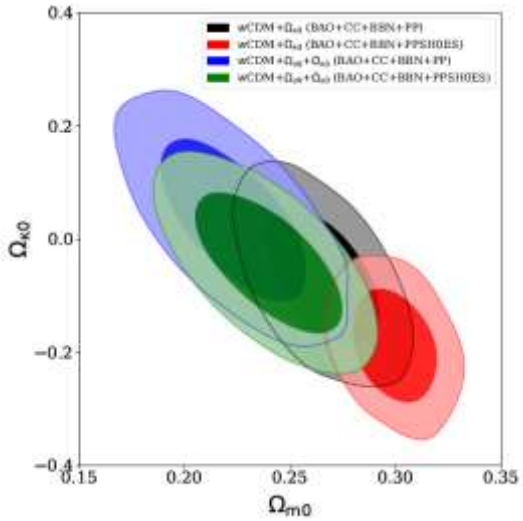

Figure 3: Two-dimensional marginalized confidence regions (at 68% and 95% CL) of Ω_{m0} - $\Omega_{\kappa 0}$ for wCDM+$\Omega_{\kappa 0}$ and wCDM+$\Omega_{\kappa 0}$ +$\Omega_{\sigma 0}$ models from BAO+CC+BBN+PP and BAO+CC+BBN+PPSHoES data combinations.

V.CONCLUSION

Comparing the extensions of ΛCDM (ΛCDM+$\Omega_{\kappa 0}$ and ΛCDM+$\Omega_{\kappa 0}$ +$\Omega_{\sigma 0}$) and wCDM (wCDM+$\Omega_{\kappa 0}$ and wCDM+$\Omega_{\kappa 0}$ +$\Omega_{\sigma 0}$) models reveal that important cosmological parameters like Ω_{m0} , H_0 are impacted by the inclusion of $\Omega_{\kappa 0}$ and $\Omega_{\sigma 0}$. Although wCDM offers greater flexibility in the dark energy equation of state, ΛCDM is still a powerful model. The Hubble tension is shown in the consistent variation in H_0 values across datasets. The universe's isotropy is supported by the extremely narrow upper bounds on $\Omega_{\sigma 0}$. Both theories are consistent with important cosmological parameters, however ${\chi^2}_{min}$ values indicate that wCDM fits somewhat better. All things considered, wCDM permits greater variance in late-time cosmic acceleration, but ΛCDM is still a strong framework for explaining the history of the universe.

VI.DATA AVAILABILITY

Publically available data are used and cited.

VII.CONFLICT OF INTEREST

The authors declare that they have no conflict of interest.

REFERENCES

1. A. Starobinsky, A new type of isotropic cosmological models without singularity, Physics Letters B 91, 99 (1980).
2. A. H. Guth, Inflationary universe: A possible solution to the horizon and flatness problems, Phys. Rev. D 23, 347 (1981).
3. A. Linde, A new inflationary universe scenario: A possible solution of the horizon, flatness, homogeneity, isotropy and primordial monopole problems, Physics Letters B 108, 389 (1982).
4. A. Albrecht and P. J. Steinhardt, Cosmology for grand unified theories with radiatively induced symmetry breaking, Phys. Rev. Lett. 48, 1220 (1982).
5. A. G. Riess and A. V. Filippenko, Observational evidence from supernovae for an accelerating universe and a cosmological constant, The Astronomical Journal 116, 1009 (1998).
6. S. Perlmutter, G. Aldering, and G. Goldhaber, Measurements of and from 42 high-redshift supernovae, The Astrophysical Journal 517, 565 (1999).
7. N. Aghanim, Y. Akrami, and M. Ashdown, Planck2018 results: Vi. cosmological parameters, Astronomy amp; Astrophysics 641, A6 (2020).
8. S. Aiola, E. Calabrese, and Maurin, The atacama cosmology telescope: Dr4 maps and cosmological parameters, Journal of Cosmology and Astroparticle Physics 2020 (12), 047–047.
9. S. Alam, M. Aubert, S. Avila, and Balland, Completed sdss-iv extended baryon oscillation spectroscopic survey: Cosmological implications from two decades of spectroscopic surveys at the apache point observatory, Physical Review D 103, 10.1103/physrevd.103.083533 (2021).
10. L. Balkenhol, D. Dutcher, et al. (SPT-3G Collaboration), Constraints on ΛCDM extensions from the spt-3g 2018 ee and te power spectra, Phys. Rev. D 104, 083509 (2021).
11. T. M. C. Abbott, M. Aguena, et al. (DES Collaboration), Dark energy survey year 3 results: Cosmological constraints from galaxy clustering and weak lensing, Phys. Rev. D 105, 023520 (2022).
12. T. M. C. Abbott, M. Aguena, et al. (DES Collaboration), Dark energy survey year 3 results: Constraints on extensions to ΛCDM with weak lensing and galaxy clustering, Phys. Rev. D 107, 083504 (2023).
13. L. Perivolaropoulos and F. Skara, Challenges for lambdacdm: An update, New Astronomy Reviews 95, 101659 (2022).
14. E. Di Valentino, W. Giar`e, A. Melchiorri, and J. Silk, Health checkup test of the standard cosmological model in view of recent cosmic microwave background anisotropies experiments, Phys. Rev. D 106, 103506 (2022).
15. E. Di Valentino, L. A. Anchordoqui, et al., Snowmass2021 - letter of interest cosmology intertwined iv: The age of the universe and its curvature, Astroparticle Physics 131, 102607 (2021).
16. E. Gazta˜naga, R. Miquel, and E. S´anchez, First cosmological constraints on dark energy from the radial baryon acoustic scale, Phys. Rev. Lett. 103, 091302 (2009).
17. M. J. Mortonson, Testing flatness of the universe with probes of cosmic distances and growth, Phys. Rev. D 80, 123504 (2009).
18. S. H. Suyu, T. Treu, et al., Cosmology from gravitational lens time delays and planck data, The Astrophysical Journal Letters 788, L35 (2014).
19. B. L'Huillier and A. Shafieloo, Model-independent test of the flrw metric, the flatness of the universe, and non-local estimation of h0 rd, Journal of Cosmology and Astroparticle Physics 2017 (01), 015.
20. A. Chudaykin, K. Dolgikh, and M. M. Ivanov, Constraints on the curvature of the universe and dynamical dark energy from the full-shape and bao data, Phys. Rev. D 103, 023507 (2021).
21. G. Acquaviva, O. Akarsu, N. Katırc ı, and J. A. Vazquez, Simple-graduated dark energy and spatial curvature, Phys. Rev. D 104, 023505 (2021).

22. G. Efstathiou, Is the low cosmic microwave background quadrupole a signature of spatial curvature?, Monthly Notices of the Royal Astronomical Society 343, L95 (2003).
23. A. D. Linde, Can we have inflation with Ω > 1?, JCAP 05, 002, arXiv:astro-ph/0303245.
24. W. Handley, Curvature tension: Evidence for a closed universe, Phys. Rev. D 103, L041301 (2021).
25. E. Di Valentino, O. Mena, S. Pan, L. Visinelli, W. Yang, A. Melchiorri, D. F. Mota, A. G. Riess, and J. Silk, In the realm of the Hubble tension—a review of solutions, Class. Quant. Grav. 38, 153001 (2021), arXiv:2103.01183 [astro-ph.CO].
26. S. Vagnozzi, E. Di Valentino, S. Gariazzo, A. Melchiorri, O. Mena, and J. Silk, The galaxy power spectrum take on spatial curvature and cosmic concordance, Physics of the Dark Universe 33, 100851 (2021).
27. G. Efstathiou and S. Gratton, The evidence for a spatially flat Universe, Monthly Notices of the Royal Astronomical Society: Letters 496, L91 (2020).
28. S. Vagnozzi, A. Loeb, and M. Moresco, Eppur `e piatto? the cosmic chronometers take on spatial curvature and cosmic concordance, The Astrophysical Journal 908, 84 (2021).
29. S. Alam, M. Aubert, et al., Completed SDSS-IV extended baryon oscillation spectroscopic survey: Cosmological implications from two decades of spectroscopic surveys at the apache point observatory, Phys. Rev. D 103, 083533 (2021).
30. S. Anselmi, M. F. Carney, J. T. Giblin, S. Kumar, J. B. Mertens, M. O'Dwyer, G. D. Starkman, and C. Tian, What is flat ΛCDM, and may we choose it?, Journal of Cosmology and Astroparticle Physics 2023 (02), 049.
31. J. N. Dossett and M. Ishak, Spatial curvature and cosmological tests of general relativity, Phys. Rev. D 86, 103008 (2012).
32. A. G. Riess, W. Yuan, et al., A comprehensive measurement of the local value of the Hubble Constant with 1kms1mpc1 uncertainty from the Hubble Space Telescope and the SH0ES Team, The Astrophysical Journal Letters 934, L7 (2022).
33. D. W. Pesce, J. A. Braatz, et al., The megamaser cosmology project. XIII. combined Hubble Constant constraints, The Astrophysical Journal Letters 891, L1 (2020).
34. J. P. Blakeslee, J. B. Jensen, C.-P. Ma, P. A. Milne, and J. E. Greene, The Hubble Constant from infrared surface brightness fluctuation distances*, The Astrophysical Journal 911, 65 (2021).
35. S. K. Choi et al., The Atacama Cosmology Telescope: a measurement of the Cosmic Microwave Background power spectra at 98 and 150 GHz, Journal of Cosmology and Astroparticle Physics 2020 (12), 045–045.
36. F. J. Qu, B. D. Sherwin, et al., The Atacama Cosmology Telescope: A Measurement of the DR6 CMB Lensing Power Spectrum and its Implications for Structure Growth (2023), arXiv:2304.05202 [astro-ph.CO].
37. D. Dutcher, L. Balkenhol, et al. (SPT-3G Collaboration), Measurements of the E-mode polarization and temperature-E-mode correlation of the CMB from SPT-3G 2018 data, Phys. Rev. D 104, 022003 (2021).
38. W. L. Freedman, Cosmology at at Crossroads: Tension with the Hubble Constant (2017), arXiv:1706.02739 [astro-ph.CO].
39. E. M¨ortsell and S. Dhawan, Does the Hubble constant tension call for new physics?, Journal of Cosmology and Astroparticle Physics 2018 (09), 025.
40. L. Knox and M. Millea, Hubble constant hunter's guide, Physical Review D 101, 10.1103/physrevd.101.043533 (2020).
41. J.-P. Hu and F.-Y. Wang, Hubble Tension: The Evidence of New Physics (2023), arXiv:2302.05709 [astro-ph.CO].
42. T. Bringmann, F. Kahlhoefer, K. Schmidt-Hoberg, and P. Walia, Converting nonrelativistic dark matter to radiation, Phys. Rev. D 98, 023543 (2018).
43. S. Kumar, R. C. Nunes, and S. K. Yadav, Cosmological bounds on dark matter-photon coupling, Phys. Rev. D 98, 043521 (2018).
44. S. K. Yadav, Constraints on dark matter-photon coupling in the presence of time-varying dark energy, Modern Physics Letters A 35, 1950358 (2019).
45. V. Yadav, S. K. Yadav, and A. K. Yadav, Observational constraints on generalized dark matter properties in the presence of neutrinos with the final planck release, Physics of the Dark Universe 42, 101363 (2023).
46. V. Poulin, T. L. Smith, T. Karwal, and M. Kamionkowski, Early dark energy can resolve the hubble tension, Phys. Rev. Lett. 122, 221301 (2019).
47. F. Niedermann and M. S. Sloth, Resolving the Hubble tension with new early dark energy, Phys. Rev. D 102, 063527 (2020).
48. J. C. Hill, E. McDonough, M. W. Toomey, and S. Alexander, Early dark energy does not restore cosmological concordance, Phys. Rev. D 102, 043507 (2020).
49. V. Poulin, T. L. Smith, and T. Karwal, The Ups and Downs of Early Dark Energy solutions to the Hubble tension: A review of models, hints and constraints circa 2023, Physics of the Dark Universe 42, 101348 (2023).
50. A. Reeves, L. Herold, S. Vagnozzi, B. D. Sherwin, and E. G. M. Ferreira, Restoring cosmological concordance with early dark energy and massive neutrinos?, Monthly Notices of the Royal Astronomical Society 520, 3688 (2023).

51. O. Akarsu, J. D. Barrow, L. A. Escamilla, and J. A. Vazquez, Graduated dark energy: Observational hints of a spontaneous sign switch in the cosmological constant, Physical Review D 101, 10.1103/physrevd.101.063528 (2020).
52. O. Akarsu, S. Kumar, E. ¨Oz¨ulker, and J. A. Vazquez, Relaxing cosmological tensions with a sign switching cosmological constant, Phys. Rev. D 104, 123512 (2021).
53. O. Akarsu, S. Kumar, E. ¨Oz¨ulker, J. A. Vazquez, and A. Yadav, Relaxing cosmological tensions with a sign switching cosmological constant: Improved results with Planck, BAO, and Pantheon data, Phys. Rev. D 108, 023513 (2023).
54. O. Akarsu, E. D. Valentino, S. Kumar, R. C. Nunes, J. A. Vazquez, and A. Yadav, ΛsCDM model: A promising scenario for alleviation of cosmological tensions (2023), arXiv:2307.10899 [astro-ph.CO].
55. S. Vagnozzi, Seven Hints That Early-Time New Physics Alone Is Not Sufficient to Solve the Hubble Tension, Universe 9, 393 (2023).
56. S. Yeung and M.-C. Chu, Directional variations of cosmological parameters from the Planck CMB data, Phys. Rev. D 105, 083508 (2022).
57. Fosalba, Pablo and Gazta˜naga, Enrique, Explaining cosmological anisotropy: evidence for causal horizons from CMB data, Monthly Notices of the Royal Astronomical Society 504, 5840 (2021).
58. Y.-Y. Wang and F. Y. Wang, Testing the isotropy of the Universe with Type Ia supernovae in a model-independent way, Monthly Notices of the Royal Astronomical Society 474, 3516 (2017).
59. J. Soltis, A. Farahi, D. Huterer, and C. M. Liberato, Percent-Level Test of Isotropic Expansion Using Type Ia Supernovae, Phys. Rev. Lett. 122, 091301 (2019).
60. D. Zhao, Y. Zhou, and Z. Chang, Anisotropy of the Universe via the Pantheon supernovae sample revisited, Monthly Notices of the Royal Astronomical Society 486, 5679 (2019).
61. O. Akarsu, S. Kumar, S. Sharma, and L. Tedesco, Constraints on a Bianchi type I spacetime extension of the standard ΛCDM model, Phys. Rev. D 100, 023532 (2019).
62. H. Amirhashchi and S. Amirhashchi, Constraining Bianchi type I universe with type Ia supernova and H(z) data, Physics of the Dark Universe 29, 100557 (2020).
63. V. Yadav, Measuring Hubble constant in an anisotropic extension of ΛCDM model, Physics of the Dark Universe 42, 101365 (2023).
64. R. J. Cooke, M. Pettini, K. M. Nollett, and R. Jorgenson, Astrophys. J. 830, 148 (2016), arXiv:1607.03900 [astro-ph.CO].
65. J. J. Bennett, G. Buldgen, P. F. De Salas, M. Drewes, S. Gariazzo, S. Pastor, and Y. Y. Y. Wong, JCAP 04, 073 (2021), arXiv:2012.02726 [hep-ph].
66. O. Akarsu, E. Di Valentino, S. Kumar, M. Ozyigit, and S. Sharma, Phys. Dark Univ. 39, 101162 (2023), arXiv:2112.07807 [astro-ph.CO].
67. C. Zhang, H. Zhang, S. Yuan, T.-J. Zhang, and Y.-C. Sun, Res. Astron. Astrophys. 14, 1221 (2014), arXiv:1207.4541 [astro-ph.CO].
68. J. Simon, L. Verde, and R. Jimenez, Phys. Rev. D 71, 123001 (2005), arXiv:astro-ph/0412269.
69. M. Moresco et al., JCAP 08, 006 (2012), arXiv:1201.3609 [astro-ph.CO].
70. A. L. Ratsimbazafy, S. I. Loubser, S. M. Crawford, C. M. Cress, B. A. Bassett, R. C. Nichol, and P. V¨ais¨anen, Mon. Not. Roy. Astron. Soc. 467, 3239 (2017), arXiv:1702.00418 [astro-ph.CO].
71. D. Stern, R. Jimenez, L. Verde, M. Kamionkowski, and S. A. Stanford, JCAP 02, 008 (2010), arXiv:0907.3149 [astro-ph.CO].
72. N. Borghi, M. Moresco, and A. Cimatti, Astrophys. J. Lett. 928, L4 (2022), arXiv:2110.04304 [astro-ph.CO].
73. K. Jiao, N. Borghi, M. Moresco, and T.-J. Zhang, Astro- phys. J. Suppl. 265, 48 (2023), arXiv:2205.05701 [astro- ph.CO].
74. M. Moresco, Mon. Not. Roy. Astron. Soc. 450, L16 (2015), arXiv:1503.01116 [astro-ph.CO].
75. R. Jimenez and A. Loeb, Astrophys. J. 573, 37 (2002), arXiv:astro-ph/0106145.
76. V. Mossa et al., Nature 587, 210 (2020).
77. D. Brout et al., Astrophys. J. 938, 110 (2022), arXiv:2202.04077 [astro-ph.CO].
78. B. Audren, J. Lesgourgues, K. Benabed, and S. Prunet, JCAP 02, 001 (2013), arXiv:1210.7183 [astro-ph.CO].
79. D. Blas, J. Lesgourgues, and T. Tram, JCAP 07, 034 (2011), arXiv:1104.2933 [astro-ph.CO].
80. https://getdist.readthedocs.io/en/latest/intro.html